PHYSICAL REVIEW B **78**, 045203 (2008)

$Ga_{1-x}Mn_xAs$/piezoelectric actuator hybrids: A model system for magnetoelastic magnetization manipulation

C. Bihler,[1,*] M. Althammer,[2,†] A. Brandlmaier,[2] S. Geprägs,[2] M. Weiler,[2] M. Opel,[2] W. Schoch,[3] W. Limmer,[3] R. Gross,[2] M. S. Brandt,[1] and S. T. B. Goennenwein[2,‡]

[1]*Walter Schottky Institut, Technische Universität München, Am Coulombwall 3, 85748 Garching, Germany*

[2]*Walther-Meissner-Institut, Bayerische Akademie der Wissenschaften, Walther-Meissner-Strasse 8, 85748 Garching, Germany*

[3]*Institut für Halbleiterphysik, Universität Ulm, 89069 Ulm, Germany*

(Received 7 April 2008; revised manuscript received 12 June 2008; published 9 July 2008)

We have investigated the magnetic properties of a piezoelectric actuator/ferromagnetic semiconductor hybrid structure. Using a GaMnAs epilayer as the ferromagnetic semiconductor and applying the piezo stress along its [110] direction, we quantify the magnetic anisotropy as a function of the voltage V_p applied to the piezoelectric actuator using anisotropic magnetoresistance techniques. As the magnetic anisotropy in GaMnAs substantially changes as a function of temperature T, the ratio of the magnetoelastic and the magnetocrystalline anistropies can be tuned from approximately 1/4 to 4. Thus, GaMnAs/piezoelectric actuator hybrids are an ideal model system for the investigation of different piezoelastic magnetization control regimes. At $T=5$ K the magnetoelastic term is a minor contribution to the magnetic anisotropy. Nevertheless, we show that the switching fields of $\rho(\mu_0 H)$ loops are shifted as a function of V_p at this temperature. At 50 K—where the magnetoelastic term dominates the magnetic anisotropy—we are able to tune the magnetization orientation by about 70° solely by means of the electrical voltage V_p applied. Furthermore, we derive the magnetostrictive constant λ_{111} as a function of temperature and find values consistent with earlier results. We argue that the piezo voltage control of magnetization orientation is directly transferable to other ferromagnetic/piezoelectric hybrid structures, paving the way to innovative multifunctional device concepts. As an example, we demonstrate piezo voltage-induced irreversible magnetization switching at $T=40$ K, which constitutes the basic principle of a nonvolatile memory element.

DOI: 10.1103/PhysRevB.78.045203 PACS number(s): 75.30.Gw, 75.50.Pp, 75.47.Pq, 77.65.−j

I. INTRODUCTION

Ferromagnetic semiconductors unite the long-range magnetic ordering characteristic of ferromagnets with the versatile properties of conventional semiconductors. This class of multifunctional materials therefore is very attractive from a fundamental physics point of view. Moreover, novel spin-electronic devices can be realized using ferromagnetic semiconductors, in which the electronic functionality is directly linked to magnetic properties such as the magnetization orientation.[1–8] For device applications it is attractive to control the magnetic properties via a *nonmagnetic* parameter. In this paper, we investigate the approach to strain a dilute magnetic semiconductor (DMS) lattice by means of an external piezoelectric actuator in order to manipulate its magnetic and magnetotransport properties. Using GaMnAs as the DMS, we discuss in detail the piezo voltage control of the magnetic anisotropy, which can be utilized to reversibly manipulate magnetization orientation, as well as to irreversibly switch the magnetization between two magnetic easy-axis orientations. The experiments discussed here pave the way for the three dimensional control of spins via a nonmagnetic control parameter.

We begin with a short introduction into GaMnAs, before reviewing different approaches to influence the magnetic properties of magnetic semiconductors via nonmagnetic parameters reported in literature. $Ga_{1-x}Mn_xAs$ is the prototype ferromagnetic semiconductor with a Curie temperature $T_C < 170$ K.[2,6,9] The strong p-d coupling between the delocalized holes and the localized electrons in the Mn d shell results in large magnetoresistive effects in GaMnAs.[10–14] Since the magnetic domains extend over 100 microns or more,[15] GaMnAs is ideally suited as a spin-injecting or spin-polarizing contact in spintronic devices. Indeed, novel functionalities or physical effects have already been demonstrated in spin-electronic devices based on GaMnAs, such as the emission of circularly polarized light from a so-called spin light emitting diode,[12,16] the controlled motion of domain walls via current pulses,[17,18] the tunneling anisotropic magnetoresistance in GaMnAs/insulator/normal metal structures,[19] and nonvolatile memory device concepts.[4,7,8]

One of the most intriguing properties of DMS is the strong dependence of their magnetic properties on nonmagnetic parameters, such as electric field,[20,21] light irradiation,[22–24] temperature,[25–27] dopant density,[28,29] strain,[30–33] or pressure.[34] This allows for various control schemes of the magnetic properties of DMS, which we shortly discuss in the following.

Ohno *et al.*[20] demonstrated that an electric field control of ferromagnetism is possible in InMnAs samples covered with a metallic gate. Electrically assisted magnetization reversal, as well as electrical demagnetization have already been demonstrated in devices utilizing this effect.[21] While this gate voltage control of ferromagnetism appears very attractive for spintronic devices, the high carrier density in degenerately doped DMS and the resulting screening effects limit the thickness of magnetic semiconductor films controllable by electric fields to a few nanometer at most, imposing severe constraints on the device geometries.

 ©2008 The American Physical Society

Another approach to vary the hole concentration and thus the magnetic properties relies on the introduction of additional nonmagnetic dopant species into GaMnAs, such as Be[28] or Al.[29] The incorporation of hydrogen also allows to control the hole density in GaMnAs.[35–37] The hydrogen incorporation is stable at ambient temperatures, but can be reversed by a mild thermal, as well as a pulsed-laser annealing.[38,39] However, while the exchange coupling in GaMnAs films with thicknesses of several hundred nanometer can be switched on or off via codoping or hydrogenation, these techniques do not allow to manipulate the magnetization orientation while operating a spintronic device.

For the realization of DMS tunable during device operation, the dependence of the magnetic properties on the crystal lattice appears much more promising. Csontos *et al.*[34] showed that the ferromagnetic exchange interaction in InMnSb can be controlled via the application of hydrostatic pressure. Also the magnetic anisotropy in GaMnAs was found to qualitatively change as a function of strain.[30–33] $Ga_{1-x}Mn_xAs$ layers grown on GaAs are compressively strained, leading to a first-order uniaxial magnetic anisotropy so that the film plane is an easy magnetic plane for the typical range of Mn concentrations $(0.01<x<0.1)$.[30–32] A smaller cubic (biaxial) anisotropy yields two approximately orthogonal easy axes within the film plane. Furthermore, a small in-plane uniaxial anisotropy along [110] is present in most GaMnAs films on GaAs,[25,26,40–46] the microscopic origin of which is still controversially discussed. In GaMnAs films with tensile strain, in contrast, the film plane is magnetically hard[30,32] so that the magnetization aligns along the film normal at low magnetic fields. Furthermore, the magnetic anisotropy in GaMnAs qualitatively changes with the temperature. In comparison to other ferromagnetic metals, demagnetization effects only play a minor role in GaMnAs, as the saturation magnetization is small due to the small concentration of magnetic ions. Recently also the control of the magnetic anisotropy via anisotropic strain relaxation in patterned structures has been reported.[47] These experimental observations are explained by the established theoretical model for the ferromagnetic exchange:[9] The strain alters the symmetry of the hole wave function in the GaAs valence band, which due to the hole mediation of ferromagnetic exchange has a strong influence on the magnetic anisotropy. This picture also is compatible with the recent measurements of the magnetoelastic constants of GaMnAs in micromechanical devices.[27]

In the following we will investigate the control of the magnetic anisotropy of GaMnAs via the application of an external stress by a piezoelectric actuator. This approach has already been shown to allow *in-situ* manipulation of magnetic anisotropy in piezoelectric actuator/ferromagnet hybrid samples at room temperature.[48,49] We have recently demonstrated that this approach can be transferred to piezoelectric actuator/GaMnAs hybrids,[50] as also reported by Refs. 51 and 52. Here we compile our extensive experimental findings and show that they can be understood consistently using a free energy model. In particular, we make use of the strong temperature dependence of the magnetic anisotropy in GaMnAs to tune the ratio of the piezo-controlled magnetoelastic and the magnetocrystalline anisotropy contribution in a range of approximately 1/4 to 4 in one and the same sample. In this way, we are able to access qualitatively different regimes: (i) At low temperatures $T\approx 5$ K, the magnetoelastic anisotropy term is small compared to the crystalline one. In this regime, the application of a voltage to the piezoelectric actuator allows to shift the switching fields of $\rho(\mu_0 H)$ loops, while the magnetization orientation is not manipulated substantially. (ii) At higher temperatures $T\gtrsim 40$ K, the magnetoelastic anisotropy is the dominant anisotropy contribution, enabling a reversible voltage control of magnetization orientation by up to 70°. Furthermore, in this regime, an irreversible, voltage-induced magnetization reorientation by up to 180° can be achieved after preparing the system by means of a magnetic field sweep. These two regimes are not particular to GaMnAs. Rather, our results show that in order to achieve a substantial piezo voltage control of magnetization orientation in any given ferromagnet/piezoelectric actuator hybrid, the ratio between magnetoelastic and magnetocrystalline anisotropies must be adjusted appropriately.

This paper is organized as follows: After a review of the magnetic free-energy approach in Sec. II, we summarize the experimental procedures employed and the properties of the piezoelectric actuator used in Secs. III and IV, respectively. The method to determine the magnetic anisotropy from magnetotransport experiments is described in Sec. V. From a comparison of the piezo-induced strain (Sec. IV) and the corresponding magnetoelastic contribution to magnetic anisotropy, we derive the temperature dependence of the magnetostrictive constant (Sec. VI). In the following sections we investigate several temperature regimes exhibiting different relative strength of the piezo-controlled magnetoelasic and the magnetocrystalline magnetic anisotropy. At low temperatures ($T\approx 5$ K) the piezo voltage-induced changes are small compared to the dominating cubic magnetic anisotropy, resulting in a piezo voltage dependence of the magnetoresistance switching fields in external magnetic field sweeps (Sec. VII). In contrast, at $T\approx 50$ K the magnetoelastic contribution dominates magnetic anisotropy (Sec. VIII), which allows to continuously and reversibly rotate magnetization orientation (Sec. IX). In Sec. X we demonstrate a piezo voltage-induced irreversible magnetization switching. After giving the conclusion in Sec. XI we discuss possible applications of the investigated effects in Sec. XII.

II. FREE ENERGY APPROACH

To describe the magnetic anisotropy and thus magnetization orientation in our sample, we adopt a free energy approach. To second order, the free energy in GaMnAs normalized to the saturation magnetization is given by[31,53,54]

$$\begin{aligned} F/M &= -\mu_0 H(\mathbf{h}\cdot\mathbf{m}) + B_{c\parallel}(m_x^4+m_y^4) \\ &\quad + B_{110}(V_p)(\mathbf{j}\cdot\mathbf{m})^2 + B_{010}m_y^2 \\ &= -\mu_0 H\cos(\beta-\alpha) \\ &\quad + B_{c\parallel}[\cos^4(\beta+45°)+\cos^4(\beta-45°)] \\ &\quad + B_{110}(V_p)\cos^2\beta + B_{010}\cos^2(\beta-45°), \end{aligned} \tag{1}$$

where we have assumed that the magnetization is aligned

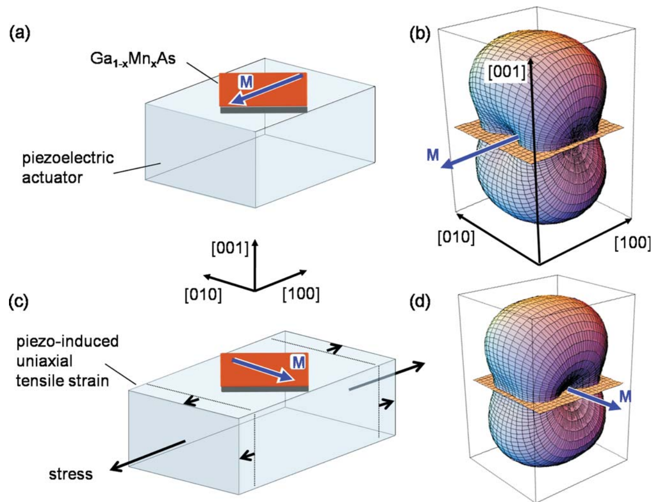

FIG. 1. (Color online) (a) Schematic illustration of a 90° magnetization switching for a GaMnAs film affixed onto a piezoelectric actuator with the magnetic easy axis [100] parallel to the main expansion direction of the actuator. (b) Corresponding free energy surface. The free energy for the magnetization oriented along a specific direction is given by the distance from the center of the coordinate system to the surface. In this example the magnetization is oriented along $[\bar{1}00]$. (c) A positive voltage applied to the actuator leads to an elongation of the actuator/GaMnAs layer. (d) This strain induces a uniaxial anisotropy with a magnetic hard axis in elongation direction, which leads to a change in the relative strength of the in-plane magnetic easy axes [Fig. 2(a)] and thus a 90° magnetization switching into the global minimum at $[0\bar{1}0]$.

within the film plane. $\mu_0 = 4\pi \times 10^{-7}$Vs/Am is the vacuum induction, m_i are the direction cosines of the magnetization relative to the cubic axes, $B_{c\|}$ is the in-plane cubic anisotropy parameter, and $B_{110}(V_p)$ and B_{010} are the uniaxial anisotropy parameters. The orientation of the external magnetic field H and the magnetization M are given by the unit vectors **h** and **m**, with the corresponding angles α and β with respect to the current direction **j** as shown in Fig. 3. The individual terms in Eq. (1) describe the Zeeman interaction, the in-plane cubic and two uniaxial magnetic anisotropy contributions along [110] and [010] crystallographic directions. The third term $[B_{110}(V_p)(\mathbf{j}\cdot\mathbf{m})^2]$, the magnetoelastic contribution to the magnetic anisotropy, accounts for the changes in magnetic anisotropy due to a voltage V_p applied to the piezoelectric actuator in the particular stress geometry discussed below. The fact that the piezo voltage-induced effect can be described by a uniaxial anisotropy is derived in the Appendix. Note that the anisotropy fields used in Refs. 55 and 56 are given by $2K_{c1}^{\|}/M = -4B_{c\|}$ for the in-plane cubic field and $2K_{u1}^{i}/M = 2B_i$ for the uniaxial fields.

Figure 1(b) illustrates a typical free energy surface of a compressively strained GaMnAs film. The free energy for the magnetization oriented along a specific direction is given by the distance from the center of the coordinate system to the surface. The magnetic anisotropy in Fig. 1(b) is dominated by a uniaxial anisotropy perpendicular to the film plane (the film plane is indicated by the orange plane). Consequently, the magnetization will be oriented within the film plane at low external fields in good approximation. In the film plane, magnetic anisotropy mainly is determined by the cubic contribution with easy axes along ⟨100⟩ at liquid He temperatures.

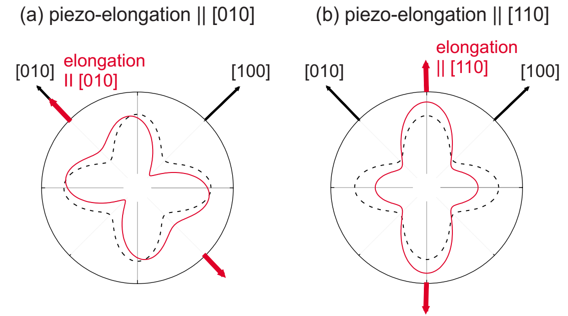

FIG. 2. (Color online) Cuts through the free energy surface within the film plane for two different strain configurations. The black dashed curves illustrate the in-plane cubic anisotropy contribution with magnetic easy axes along ⟨100⟩. (a) For the main elongation direction of the piezoelectric actuator aligned along a magnetic easy axis, the strain-induced uniaxial anisotropy leads to a change of the relative strengths of the magnetic easy axes (red full curve). (b) In contrast, for the main elongation direction of the piezoelectric actuator aligned along a locally hard axis of the in-plane cubic anisotropy, e.g., [110], the strain-induced uniaxial anisotropy leads to a rotation and a change of the relative orientations of the magnetic easy axes (red full curve).

To achieve a piezo control of the magnetization orientation, the GaMnAs film is cemented onto the piezoelectric actuator (Sec. III). Regarding the relative orientation of the GaMnAs film and the main elongation direction of the piezoelectric actuator there are two qualitatively different approaches: (i) To achieve an irreversible switching of the magnetization from one minimum of cubic anisotropy into another, the GaMnAs film has to be affixed onto the piezoelectric actuator with an easy axis parallel to the main expansion direction of the actuator [Fig. 1(a)].[52] In this way, starting from a GaMnAs film magnetized along the main expansion direction, the application of a positive voltage will lead to tensile strain and thus induce a uniaxial magnetoelastic contribution with a magnetic hard axis along the expansion direction [Fig. 1(c)]. Thereby, the magnetization can be switched by 90° into the direction of the new global minimum in free energy surface [Figs. 1(d) and 2(a)]. We note that two equivalent global minima are present at [010] and $[0\bar{1}0]$. In order to lift this degeneracy, e.g., a small external magnetic field should be applied in experiment. (ii) In contrast, to be able to continuously and reversibly rotate magnetization within the film plane, we here will affix the GaMnAs film onto the piezo actor with the orientation of the [110] sample edge parallel to the main expansion direction (Fig. 3). The difference between these two approaches can be visualized via cuts through the free energy surface within the film plane (Fig. 2). While in the alignment (i) [Fig. 2(a)] the relative strength of the magnetic easy axes is changed, the alignment (ii) [Fig. 2(b)] allows a rotation and thus a change of the relative orientation of the magnetic easy axes.

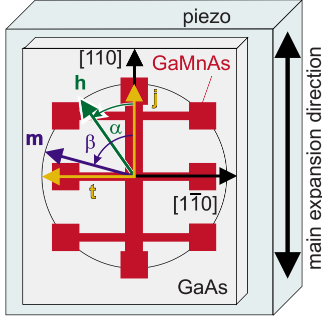

FIG. 3. (Color online) Illustration of the relative alignment of the Hall bar, the GaMnAs thin film, and the main expansion direction of the piezoelectric actuator. $\mathbf{h}=\mathbf{H}/H$, $\mathbf{m}=\mathbf{M}/M$, $\mathbf{j}$, and $\mathbf{t}$ denote the unit vectors along the orientation of the magnetic field H, the magnetization M, the current density j, and the direction transverse to the current, respectively.

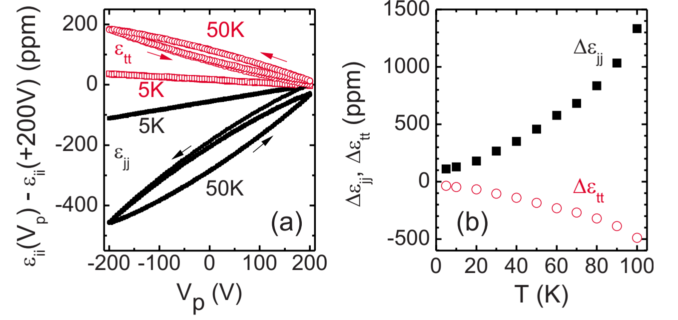

FIG. 4. (Color online) (a) Longitudinal (ϵ_{jj}, black full symbols) and transverse (ϵ_{tt}, red open symbols) lattice distortions for piezo voltage sweeps at 5 K (squares) and 50 K (circles) determined via strain gauges. The data show three full voltage cycles. To allow for comparison, we plot $\epsilon_{ii}(V_p)-\epsilon_{ii}(+200\text{ V})$, $i\in\{j,t\}$. (b) Temperature dependence of the piezo-induced lattice distortions $\Delta\epsilon_{ii}=\epsilon_{ii}(V_p=+200\text{ V})-\epsilon_{ii}(V_p=-200\text{ V})$, $i\in\{j,t\}$, determined from the third voltage cycle.

III. EXPERIMENT

The 30-nm-thick $Ga_{1-x}Mn_xAs$ film with a Mn concentration $x=0.045$ investigated here was grown on a (001)-oriented GaAs substrate by low-temperature molecular-beam epitaxy (LT-MBE).[53] The sample exhibits a Curie temperature $T_C\approx 85$ K determined from superconducting quantum interference device (SQUID) magnetometry. Via optical lithography and wet chemical etching, we patterned the film into Hall bars with the current direction $\mathbf{j}$ along the [110] crystal axis. After the etching process the GaAs substrate was mechanically polished to a thickness of about 100 μm. The sample then was cemented onto a lead zirconate titanate (PZT) piezoelectric actuator "PSt 150/2×3/5*a*" (Piezomechanik München) using the two-component epoxy "M-Bond 600" (Vishay Inc.) annealed for 2 h at 120 °C in air. As shown in Fig. 3 the main piezoelectric actuator expansion direction is aligned parallel to the GaAs [110] direction.

We extracted the magnetic anisotropy from magnetotransport experiments carried out in a superconducting magnet cryostat. The sample was mounted on a rotatable sample stage that allows rotation around one axis, in such a way that the applied magnetic field always lay within the film plane, and that the angle α enclosed by the magnetic field orientation $\mathbf{h}$ and the current density $\mathbf{j}$ could be adjusted within $-140°<\alpha<140°$, as illustrated in Fig. 3. Using a dc current density of $j=4.4\times10^3$ A cm^{-2} the resistivities ρ_{long} along $\mathbf{j}$ and ρ_{trans} perpendicular to $\mathbf{j}$ were recorded via four-point measurements. We studied the magnetic properties of the sample using conventional magnetoresistance traces $\{\rho_{\text{long}}(\mu_0H),\rho_{\text{trans}}(\mu_0H)\}$ at a fixed magnetic field orientation α, as well as via angle-dependent magnetoresistance (ADMR) measurements $\{\rho_{\text{long}}(\alpha),\rho_{\text{trans}}(\alpha)\}$ at a fixed external magnetic field strength.

IV. MEASUREMENT OF PIEZO-INDUCED STRAIN

Application of a positive piezo voltage results in a lattice elongation ϵ_{jj} along $\mathbf{j}$ and a lattice contraction ϵ_{tt} along $\mathbf{t}$ perpendicular to $\mathbf{j}$ (cf. Fig. 3). To determine the temperature dependence of the piezo-induced lattice distortions $\epsilon_{ii}(V_p)$, $i\in\{j,t\}$, we used strain gauges. Figure 4(a) depicts the measured longitudinal (ϵ_{jj}) and transverse (ϵ_{tt}) lattice distortions for piezo voltage sweeps at 5 K and 50 K. For increasing temperature we observe an increase in both the total lattice distortions $\Delta\epsilon_{ii}=\epsilon_{ii}(V_p=+200\text{ V})-\epsilon_{ii}(V_p=-200\text{ V})$, $i\in\{j,t\}$ [Fig. 4(b)] and the hysteresis exhibited by the piezoelectric actuator [Fig. 4(a)]. This piezo voltage-induced strain causes an additional magnetoelastic contribution $F_{\text{magel}}(V_p)/M=B_{110}(V_p)\cos^2\beta$ to the magnetic anisotropy as derived in the Appendix. Positive (negative) piezo voltage thus results in an additional uniaxial magnetic anisotropy with a magnetic hard (easy) axis along $\mathbf{j}$ direction.

V. DETERMINATION OF MAGNETIC ANISOTROPY FROM MAGNETOTRANSPORT

We now describe the determination of the magnetic anisotropy from magnetotransport measurements, in which the external magnetic field H is rotated at different field strengths within the film plane, as introduced above. Due to the dominating uniaxial anisotropy in growth direction caused by epitaxial strain, the magnetization in our film, in good approximation, is aligned within the film plane. Therefore, the longitudinal and the transverse resistivities

$$\rho_{\text{long}}=\rho_0+\rho_1(\mathbf{j}\cdot\mathbf{m})^2+\rho_3(\mathbf{j}\cdot\mathbf{m})^4 = \rho_0+\rho_1\cos^2\beta+\rho_3\cos^4\beta, \quad (2)$$

$$\rho_{\text{trans}}=\rho_7(\mathbf{t}\cdot\mathbf{m})(\mathbf{j}\cdot\mathbf{m})=\frac{1}{2}\rho_7\sin(2\beta) \quad (3)$$

are determined by the angle β between the in-plane orientation of the magnetization $\mathbf{m}$ and the current direction $\mathbf{j}$. The orientation $\mathbf{t}$ denotes the in-plane direction perpendicular to $\mathbf{j}$ (Fig. 3). These expressions can be derived from a series expansion of the resistivity tensor in powers of the magnetization components m_i.[3,54] Following Limmer *et al.*[53,54] the resistivity parameters ρ_0, ρ_1, ρ_3, and ρ_7 can be deduced from magnetotransport measurements in which a constant large

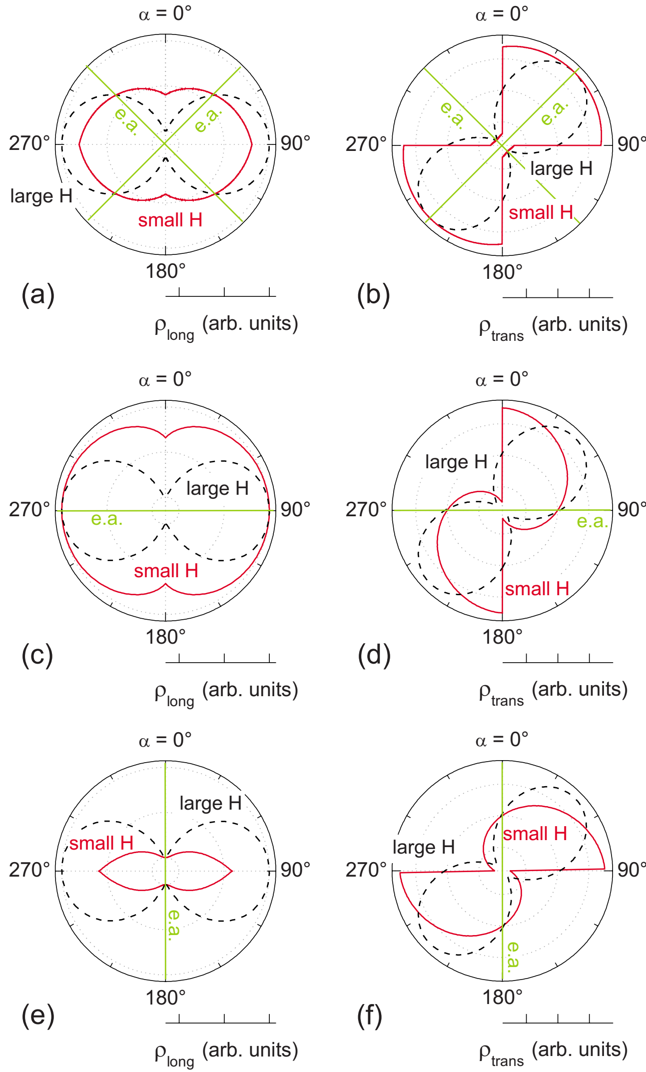

FIG. 5. (Color online) Schematic illustration of ADMR according to Eqs. (2) and (3). In all panels, the same ρ_0, $\rho_7>0$ and ρ_1, $\rho_3<0$ have been used. The black dashed curves correspond to $\{\rho_{\mathrm{long}}(\alpha),\rho_{\mathrm{trans}}(\alpha)\}$ curves for a large magnetic field H rotated within the film plane, so that the magnetization is aligned in field direction, i.e., $\beta=\alpha$. For small magnetic fields H, the magnetization tends to remain oriented close to a magnetic easy axis (e.a., green straight lines) and ρ_{long} and ρ_{trans} therefore tend to remain constant over a broad range of external magnetic field orientations nearby a magnetic easy axis, resulting in $\{\rho_{\mathrm{long}}(\alpha),\rho_{\mathrm{trans}}(\alpha)\}$ given by the red full curves. (a), (b) represent the case of a cubic magnetic anisotropy in the film plane, while in (c), (d) [(e), (f)] an in-plane uniaxial anisotropy with the easy axis along 90° [0°] is present. Note that this figure shows the relevant ADMR features, which will be observed as a function of temperature in Figs. 6 and 11.

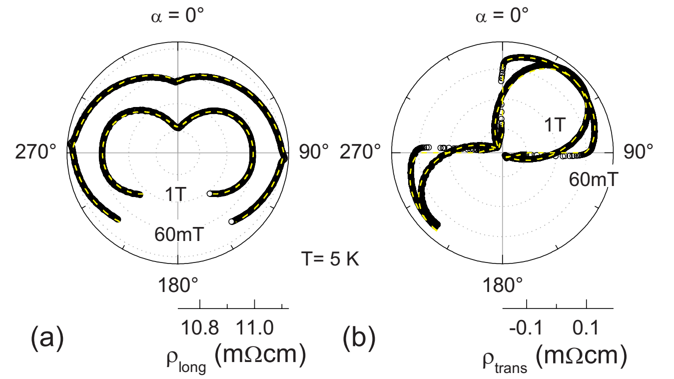

FIG. 6. (Color online) (a) Longitudinal resistivity $\rho_{\mathrm{long}}(\alpha)$ and (b) transverse resistivity $\rho_{\mathrm{trans}}(\alpha)$ for a constant external magnetic field $\mu_0H=60$ mT and 1 T rotated within the film plane for $V_p=0$ V. The black circles represent the experimental data, the yellow dashed curves the result of the corresponding simulation using the parameter values given in Fig. 7.

external magnetic field H is rotated in the film plane. In good approximation, the magnetization in this case can be assumed to be oriented along the magnetic field direction, i.e., $\beta=\alpha$ in Eq. (2) and (3), where α denotes the angle between the magnetic-field orientation $\mathbf{h}$ and the current direction $\mathbf{j}$. Equations (2) and (3) then yield the black dashed curves for $\{\rho_{\mathrm{long}}(\alpha),\rho_{\mathrm{trans}}(\alpha)\}$ in Fig. 5. Note that angles are defined in the mathematically positive sense (counterclockwise) in Fig. 3 and are plotted clockwise in the following. Thus +90° corresponds to the $[\bar{1}10]$ direction and not $[1\bar{1}0]$ as given in Ref. 50. In contrast, for measurements at smaller external magnetic fields, the orientation of magnetization—and also ρ_{long} and ρ_{trans}—to an increasing extent will be influenced by the magnetic anisotropy. Therefore, at small magnetic fields the magnetization will tend to remain oriented close to a magnetic easy axis (e.a., depicted as green straight lines in Fig. 5)—and ρ_{long} and ρ_{trans} will tend to remain constant—over a broad range of external magnetic-field orientations near to a magnetic easy axis. Accordingly, abrupt changes in $\{\rho_{\mathrm{long}}(\alpha),\rho_{\mathrm{trans}}(\alpha)\}$ indicate a nearby magnetic hard axis, as shown by the red full curves in Fig. 5. This is true for both a dominant in-plane cubic magnetic anisotropy [as is the case for GaMnAs at liquid He temperature, Figs. 5(a) and 5(b)], as well as a dominant in-plane uniaxial magnetic anisotropy [as is the case at higher $T<T_C$, Figs. 5(c)–5(f)]. Note that a similar approach to determine the in-plane magnetic anisotropy in GaMnAs has recently been followed by Yamada *et al.*[57]

For the angle-dependent magnetoresistance (ADMR) measurements, we first aligned the magnetization into a well-defined initial state in an external magnetic field of $\mu_0H=7$ T along $\alpha=-140°$. Then, we lowered the field to the measurement field and started the angular scan $\{\rho_{\mathrm{long}}(\alpha),\rho_{\mathrm{trans}}(\alpha)\}$. Figure 6 shows $\{\rho_{\mathrm{long}}(\alpha),\rho_{\mathrm{trans}}(\alpha)\}$ measured at $T=5$ K and $V_p=0$ V for rotations within external magnetic fields μ_0H of 1 T and 60 mT. Following the discussion above, the angular dependence at small μ_0H already indicates that the in-plane anisotropy is dominated by a cubic contribution with magnetic easy axes along $\langle 100\rangle$ [compare Figs. 5(a) and 5(b)]. This is corroborated by the simulation, where the simulated curves (yellow dashed) are the result of a procedure in which the resistivity parameters and the anisotropy parameters from Eq. (1) are fitted iteratively.[53] The values for ρ_0, ρ_1, ρ_3, and ρ_7 and the anisotropy fields thus obtained are summarized in Fig. 7 below. We note that in this fit all resistivity parameters except for ρ_0 are kept constant for the different values of the applied magnetic field. The

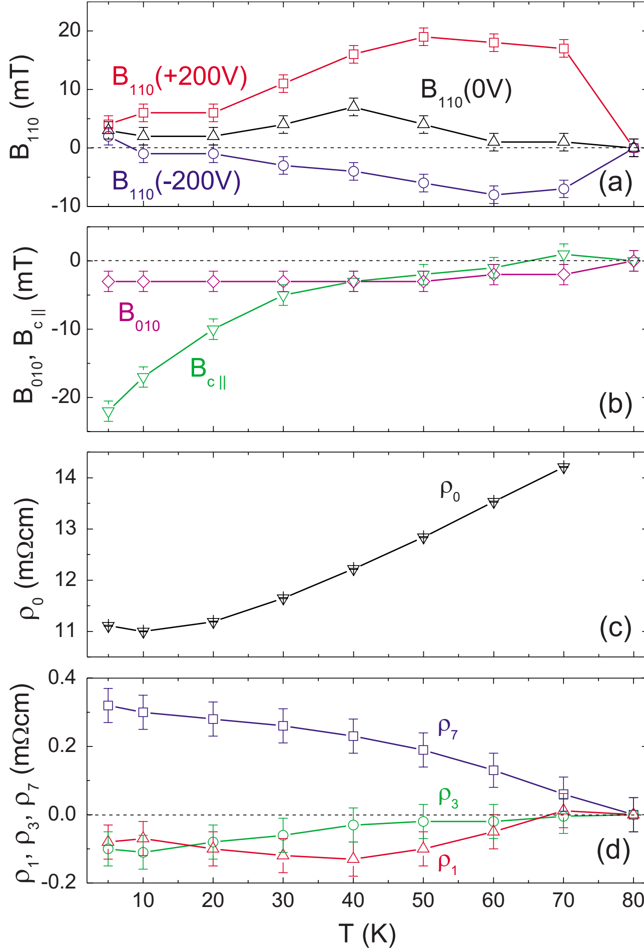

FIG. 7. (Color online) Temperature dependence of the anisotropy parameters $B_{110}(V_p)$, B_{010}, and $B_{c\|}$ (a), (b) and the resistivity parameters ρ_0, ρ_1, ρ_3, and ρ_7 (c), (d) as derived from the iterative fitting procedure of the ADMR curves at different external magnetic field strengths. At temperatures $T \lesssim T_C/2 \approx 40$ K the magnetic anisotropy is dominated by the cubic contribution, while at higher temperatures $T \gtrsim T_C/2$ the piezo voltage-induced uniaxial magnetic anisotropy contribution becomes more important. Parameter ρ_0 in (c) was derived from measurements at $V_p = +200$ V and $\mu_0 H = 100$ mT, the parameters ρ_1, ρ_3, and ρ_7 are found to be independent of V_p within error bars.

change in ρ_0 with magnetic field strength accounts for the influence of negative magnetoresistance typically observed for GaMnAs.[58]

VI. TEMPERATURE DEPENDENCE OF THE MAGNETIC ANISOTROPY AND THE MAGNETOSTRICTIVE CONSTANT

From the full set of ADMR $\{\rho_{\text{long}}(\alpha), \rho_{\text{trans}}(\alpha)\}$ measurements and the corresponding analyses for $V_p \in \{+200\text{ V}, 0\text{ V}, -200\text{ V}\}$ at different temperatures (cf. Sec. VIII for $T=50$ K), we obtain the temperature dependence of the resistivity parameters ρ_0, ρ_1, ρ_3, and ρ_7 and the anisotropy parameters $B_{110}(V_p)$, B_{010}, and $B_{c\|}$ (shown in Fig. 7). Within error bars we did not observe a dependence of ρ_1, ρ_3, and ρ_7 on V_p. The dependence of the resistivity parameters on the external magnetic field has recently been investigated by Wu *et al.*[59] in the range $0.5\text{ T} \le \mu_0 H \le 9$ T. For the magnetic field range $\mu_0 H \le 1$ T of our ADMR measurements, we also did not observe a magnetic field dependence of ρ_1, ρ_3, and ρ_7, which within error bars is in agreement with Ref. 59. The piezo voltage dependence of ρ_0 at 50 K is exemplarily shown in Figs. 13(a) and 13(c).

As typically observed for GaMnAs, the magnetic anisotropy at low temperatures ($T \lesssim T_C/2 \approx 40$ K) is dominated by the cubic magnetic anisotropy contribution. In this temperature regime the magnetoelastic anisotropy is only about 1/4 of the magnetocrystalline one [Figs. 7(a) and 7(b)]. As we will discuss in Sec. VII in this regime application of voltage on the piezoelectric actuator allows shifting the switching fields in $\rho(\mu_0 H)$ curves. At higher temperatures ($T \gtrsim T_C/2$) the cubic anisotropy term strongly decreases so that magnetocrystalline anisotropy is dominated by the uniaxial contribution. Simultaneously the magnetoelastic anisotropy contribution substantially increases due to the increase in the absolute piezo elongation with temperature (Fig. 4). Thus, in this temperature range the magnetoelastic term $B_{110}(\pm 200\text{ V})$ is about a factor of four larger than the magnetocrystalline one. This enables the substantial piezo voltage control of magnetization orientation, as will be discussed in Secs. IX and X.

In the following we use the magnetic anisotropy constants $B_{c\|}$, B_{010}, and B_{110}, as derived from the analysis of the magnetotransport measurements (Fig. 7) and the piezo-induced lattice distortion (Fig. 4) to derive the magnetostrictive constant λ_{111}. In contrast to B_{110}, this quantity is a property of the GaMnAs film and not dependent on the particular method used to apply stress. As detailed in the Appendix, the magnetostrictive constant $\lambda_{111}(T)$ can be calculated from

$$\lambda_{111}(T) = \frac{2\Delta B_{110}(T) M(T)}{3c_{44}[\Delta\epsilon_{jj}(T) - \Delta\epsilon_{tt}(T)]}, \tag{4}$$

using the temperature dependence of the piezo-induced lattice distortions $\Delta\epsilon_{ii} = \epsilon_{ii}(V_p = +200\text{ V}) - \epsilon_{ii}(V_p = -200\text{ V})$, $i \in \{j,t\}$ (Fig. 4), of $\Delta B_{110}(T) = B_{110}(T, V_p = +200\text{ V}) - B_{110}(T, V_p = -200\text{ V})$ [Fig. 7(a)], and of the magnetization $M(T)$ determined via superconducting quantum interference device (SQUID) magnetometry at a fixed magnetic field strength of $\mu_0 H = 100$ mT. For c_{44}, we use the elastic modulus of bulk GaAs. Since it only varies slightly with temperature, a fixed value of $c_{44} = 59.9$ GPa (Ref. 60) is used in all calculations. The temperature dependence observed is summarized in Fig. 8 and compared to the results of Masmanidis *et al.*[27] To our knowledge, this is only the second time that this quantity is measured for GaMnAs. Around 10 K to 20 K there is good agreement with the values obtained via nanoelectromechanical measurements. Due to the small magnetoelastic contribution to the magnetic anisotropy at 5 K, we do not attribute a high significance to our data point at this low temperature. The deviation at higher temperatures between our data and Ref. 27 can be accounted for by the differences in T_C between the 80 nm thick $Ga_{0.948}Mn_{0.052}As$ sample in Ref. 27 with $T_C = 57$ K and our 30-nm-thick $Ga_{0.955}Mn_{0.045}As$ sample with a much higher $T_C = 85$ K.

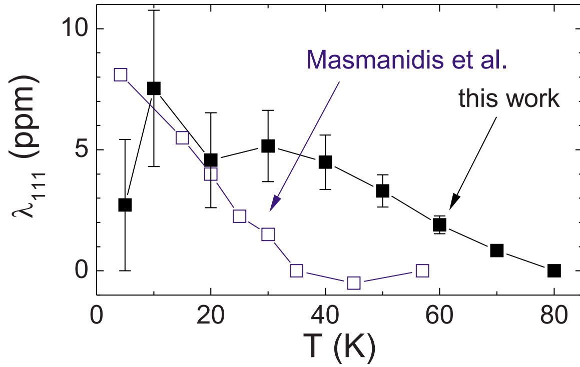

FIG. 8. (Color online) Temperature dependence of the magnetostrictive constant (full black squares) compared to the values obtained by Masmanidis *et al.*(Ref. 27) via a nanoelectromechanical resonator (open blue squares).

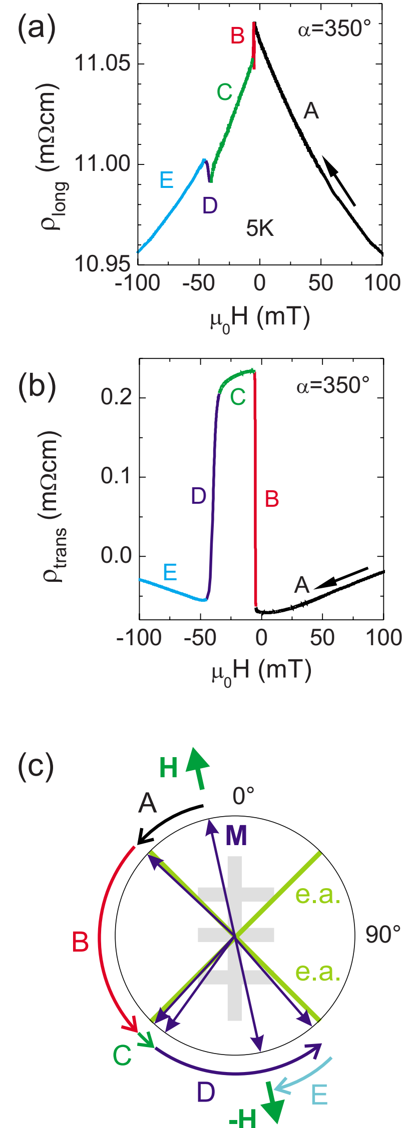

FIG. 9. (Color online) (a) $\rho_{long}(\mu_0 H)$ and (b) $\rho_{trans}(\mu_0 H)$ curves measured at 5 K for the external magnetic field H aligned at $\alpha=350°$. An explanation of the evolution is given in the text. (c) Illustration of the evolution of magnetization orientation during the external magnetic field sweep.

VII. ADMR AND PIEZO STRAIN AT 5 K

At 5 K the influence of piezo-induced strain on the ADMR scans $\{\rho_{long}(\alpha),\rho_{trans}(\alpha)\}$ discussed in Sec. V is only marginal. This is due to the small piezo-induced lattice distortion at 5 K (Fig. 4) and the large cubic anisotropy (Fig. 7) at this temperature. However, the influence of the magnetoelastic contribution can be resolved in conventional $\{\rho_{long}(\mu_0 H),\rho_{trans}(\mu_0 H)\}$ magnetotransport measurements.

Figure 9 shows the $\{\rho_{long}(\mu_0 H),\rho_{trans}(\mu_0 H)\}$ downsweep curves measured at 5 K for the external magnetic field H aligned at $\alpha=350°$. The evolution of the downsweep curve for $V_p=0$ V from positive to negative magnetic fields can be understood as follows (compare the corresponding evolution of $\{\rho_{long}(\alpha),\rho_{trans}(\alpha)\}$ in Fig. 6 at $\mu_0 H=1$ T where $\beta=\alpha$ is fulfilled): (A) $\mu_0 H=+100$ mT$\rightarrow -5$ mT: rotation of magnetization from $\beta=350°\rightarrow 315°$, the orientation of the closest magnetic easy axis. (B) $\mu_0 H=-5$ mT: first switching process by $\Delta\beta\approx 90°$ into a direction close to the magnetic easy axis at 225°. We refer to the corresponding field as a switching field in the following. This magnetization switching process can be limited by either domain nucleation or domain wall propagation. While we have no microscopic evidence, the magnetoresistance data—and in particular the dependence of the switching fields on the strain (Fig. 10)—can be consistently understood in terms of domain nucleation, as discussed in more detail in the next paragraph. We therefore favor this mechanism. In contrast, domain wall propagation would be limited by the presence of pinning centers, which should not significantly be affected by strain. (C) $\mu_0 H=-5$ mT$\rightarrow -40$ mT: slight rotation of the magnetization (corresponding to a decrease in β) within the minimum of free energy close to 225°. (D) $\mu_0 H=-40$ mT: second switching process by $\Delta\beta\approx 90°$ into a direction close to the magnetic easy axis at 135°. (E) $\mu_0 H=-40$ mT$\rightarrow -100$ mT: rotation of magnetization from $\beta\approx 135°\rightarrow 170°$, the orientation of the external magnetic field. Note that the change in $\{\rho_{long}(\mu_0 H),\rho_{trans}(\mu_0 H)\}$ during each step [(A) to (E)] of the downsweep described above is in agreement with the values expected for the corresponding orientation of magnetization from the angle-dependent resistivity loops $\{\rho_{long}(\alpha),\rho_{trans}(\alpha)\}$ at high external magnetic field in Fig. 6, where $\beta=\alpha$ is fulfilled. For example, this comparison explains the fact that the jumps observed in ρ_{trans} are much larger than the ones observed in ρ_{long}, since for the first switching process (B) ρ_{trans} jumps from its minimum value at 315° to its maximum value at 225°, while ρ_{long} exhibits exactly the same values at 315° and 225°. The fact that ρ_{long} nonetheless decreases at (B) for decreasing $\mu_0 H$ indicates that the magnetization does not exactly switch from $\beta=315°$ to $\beta=225°$, but from $\beta=315°-\epsilon_1$ to $\beta=225°-\epsilon_2$ $(\epsilon_1,\epsilon_2\gtrsim 0°)$, as depicted in Fig. 9(c).

Figures 10(c) and 10(a) shows the dependence of the first (B) and the second (D) switching field on V_p for the same magnetic-field orientation $\alpha=350°$. For positive (negative) V_p the first switching field shifts to lower (higher) and the second switching field to higher (lower) absolute values of the magnetic field. This observation can be explained via a

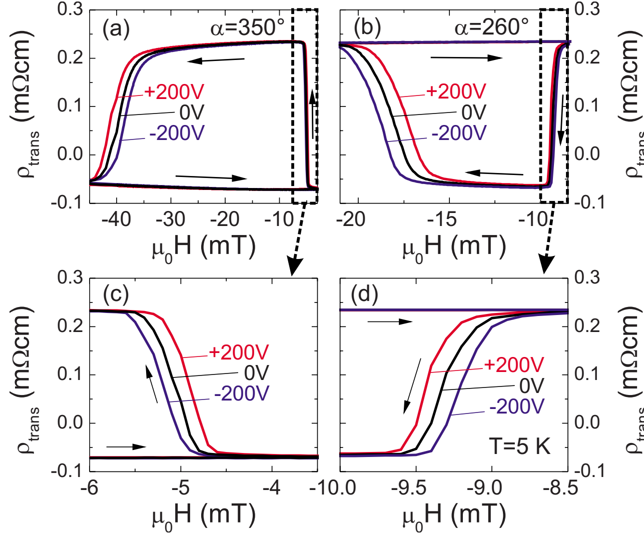

FIG. 10. (Color online) (a), (c) Enlarged sections of the $\rho_{trans}(\mu_0 H)$ curves measured at 5 K for the external magnetic field H aligned at $\alpha=350°$ showing the piezo voltage dependence of the first (c) and second (a) switching field. (b), (d) For $\alpha=260°$ the order of switching fields depending on the piezo voltage is inverted. The arrows indicate the direction of the field sweeps.

slight tilt of the relative orientation of the magnetic easy axes. A positive V_p induces a uniaxial magnetic anisotropy with a magnetic hard axis along **j**, leading to a switching angle $<90°$ for the first and $>90°$ for the second switching process. The smaller the switching angle, the smaller is the energy cost for the domain nucleation process, which in turn is determined by the energy cost for the domain wall formation around a new magnetic domain nucleus. The latter has to be accounted for by the energy gain of the magnetization switching into the energetically more favorable minimum in free energy. Therefore, a smaller (larger) angle between two magnetic easy axes leads to a shift of the corresponding switching field to smaller (larger) absolute values of the magnetic field, in agreement with experimental observation. For the external magnetic field aligned along $\alpha=350°-90°=260°$, the order of the switching fields is inverted compared to $\alpha=350°$ [Figs. 10(b) and 10(d)]. This is due to the fact that the order of the switching angles is inverted, too, corroborating our analysis.

VIII. ADMR AND PIEZO STRAIN AT 50 K

Due to the strong temperature dependence of magnetic anisotropy in GaMnAs (Secs. I and VI), the magnetic anisotropy landscape can be adjusted to a regime in which piezo voltage-induced strain qualitatively alters magnetic anisotropy.[50] This becomes obvious from the $\{\rho_{long}(\alpha),\rho_{trans}(\alpha)\}$ ADMR measurements at 50 K (Fig. 11). For $\mu_0 H=100$ mT, the magnetization orientation is still predominantly determined by the orientation of the external magnetic field α. Therefore, at $\mu_0 H=100$ mT the $\{\rho_{long}(\alpha),\rho_{trans}(\alpha)\}$ curves at different piezo voltages only exhibit minor changes. However, for $\mu_0 H=10$ mT, the magnetization orientation and thus also the magnetic anisotropy is

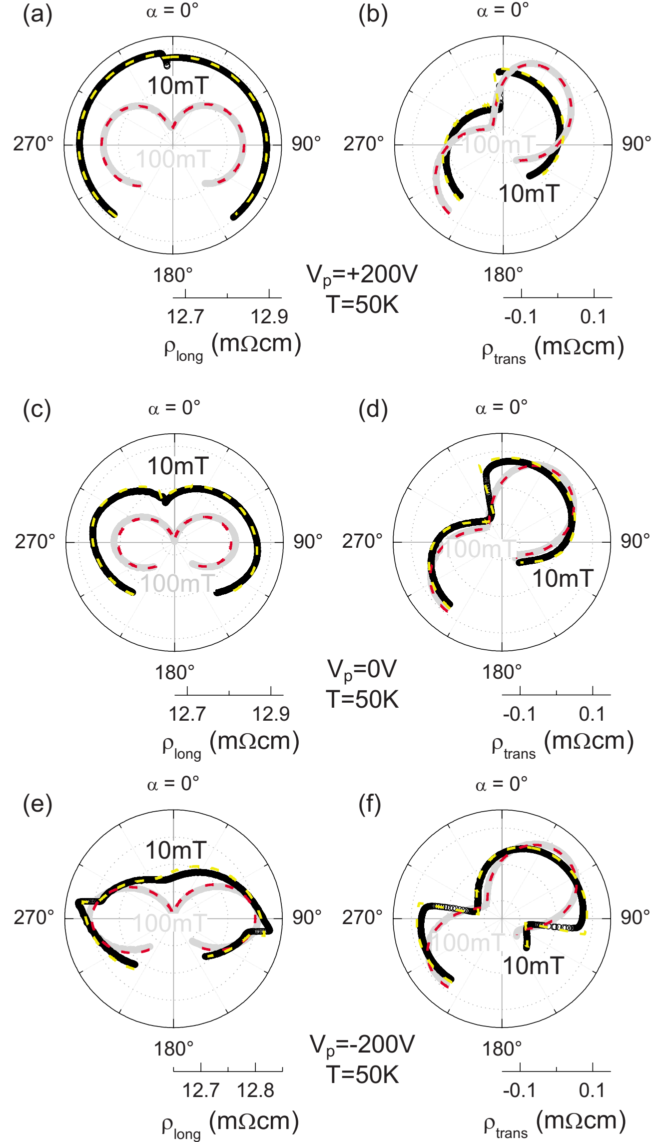

FIG. 11. (Color online) Longitudinal resistivity $\rho_{long}(\alpha)$ and transverse resistivity $\rho_{trans}(\alpha)$ at 50 K for a constant external magnetic field rotated within the film plane at different voltages V_p applied to the piezoelectric actuator: (a), (b) $V_p=+200$ V, (c),(d) $V_p=0$ V, and (e), (f) $V_p=-200$ V. The black and gray symbols correspond to the ADMR curves obtained at $\mu_0 H=10$ mT and $\mu_0 H=100$ mT, respectively. The yellow ($\mu_0 H=10$ mT) and red ($\mu_0 H=100$ mT) dashed curves are obtained from the iterative fitting procedure of the ADMR curves at different external magnetic field strengths using the parameter values given in Fig. 7.

strongly influenced by the piezo-induced strain, which can be deduced from the qualitatively different behavior of $\{\rho_{long}(\alpha),\rho_{trans}(\alpha)\}$ at different piezo voltages. As shown in Figs. 11(a) and 11(b) for an external magnetic field of 10 mT at $V_p=+200$ V, ρ_{long} and ρ_{trans} exhibit abrupt changes for an angle of the magnetic field $\alpha\approx 0°$ between **h** and **j**, indicating a nearby magnetic hard axis. The smooth changes in resistivity around $\alpha\approx 90°$ indicate a nearby magnetic easy axis [compare Figs. 5(c) and 5(d)]. In contrast, the curvature for $V_p=-200$ V [Figs. 11(e) and 11(f)] evolves approximately vice versa, indicating a rotation of the magnetic easy

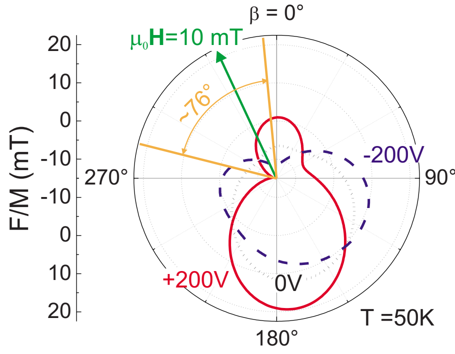

FIG. 12. (Color online) Free energy normalized to the saturation magnetization $F/M(\beta)$ as a function of magnetization orientation β for an external magnetic field $\mu_0 H = 10$ mT applied along $\alpha = -25°$ taking into account the magnetic anisotropy parameters derived from the ADMR at different magnetic field strengths at 50 K depicted in Fig. 11. The magnetization orientation is expected to change by $\Delta\beta = 76°$ when the piezo voltage V_p is varied between +200 V and −200 V.

axis by almost 90° [compare Figs. 5(e) and 5(f)]. In a more thorough analysis the anisotropy parameters are determined independently for each piezo voltage via the iterative fitting procedure of the ADMR curves at different external magnetic field strengths, as already described above for the measurements at 5 K (Sec. V). In this way we are able to quantitatively determine the piezo voltage-induced change in the free energy surface at $T = 50$ K. This analysis yields a rotation of the magnetic easy axis by about 70°.

IX. REVERSIBLE PIEZO VOLTAGE CONTROL OF MAGNETIZATION ORIENTATION

As discussed in the preceding section we are able to rotate the orientation of the magnetic easy axis by about 70° via the application of different piezo voltages at 50 K. However, since at zero external magnetic field the magnetization can decay into magnetic domains aligned either parallel or antiparallel to the magnetic easy axis, a piezo voltage control of magnetization orientation is not granted. To prevent this issue of domain formation, we apply a small external magnetic field fixed at $\alpha = -25°$, which lifts the degeneracy between antiparallel and parallel alignments of **m** relative to the magnetic easy axis. In this way only one global free energy minimum prevails, which is oriented along $\beta = -80°$ for $V_p = +200$ V and along $\beta = -5°$ for $V_p = -200$ V for $\mu_0 H = 10$ mT (Fig. 12).

We now take advantage of the direct correspondence between $\{\rho_{\mathrm{long}}, \rho_{\mathrm{trans}}\}$ and the magnetization orientation to *in-situ* monitor the evolution of magnetization orientation as a function of V_p. A measurement of $\rho_{\mathrm{long}}(V_p)$ and $\rho_{\mathrm{trans}}(V_p)$ allows to recalculate the corresponding magnetization orientation $\beta(V_p)$ via inversion of Eqs. (2) and (3). For details regarding the inversion we refer to Ref. 50. Since the data obtained for $\mu_0 H = 10$ mT applied along $\alpha = -25°$ have already been discussed in detail in Ref. 50, in the following we will focus on the changes observed for different external magnetic field strengths. Figures 13(a) and 13(b) [(c), (d)]

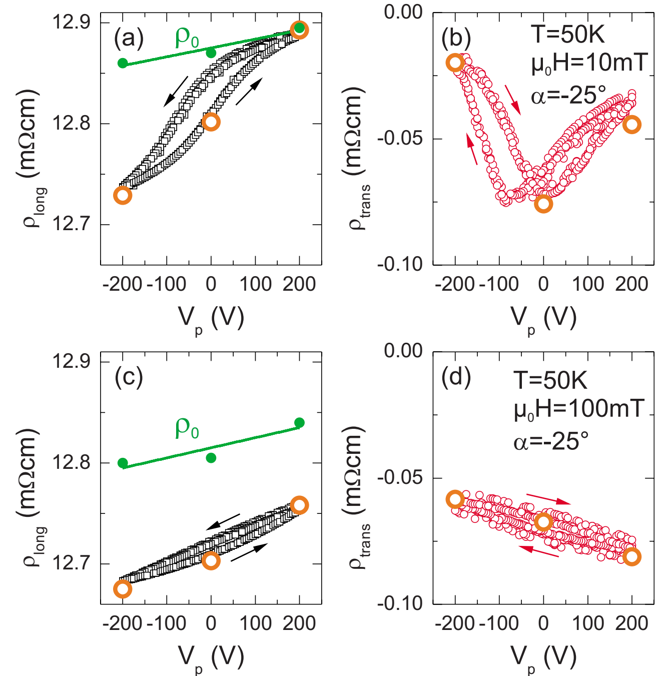

FIG. 13. (Color online) Evolution of (a) $\rho_{\mathrm{long}}(V_p)$ and (b) $\rho_{\mathrm{trans}}(V_p)$ as a function of the variation of the piezo voltage V_p between +200 V and −200 V for $\mu_0 H = 10$ mT applied along $\alpha = -25°$ at 50 K. The solid green line in (a) displays the elongation dependence of the resistivity parameter ρ_0 in ρ_{long} [compare Eq. (2)] as derived from the corresponding ADMR curve, which is subtracted from ρ_{long} for the magnetization orientation determination. (c),(d) Corresponding measurements for $\mu_0 H = 100$ mT. In all panels the orange open circles at $V_p = -200$ V, 0 V, and +200 V display the resistivity values obtained from the ADMR measurements at $\alpha = -25°$ (cf. Fig. 11), demonstrating the good reproducibility.

show $\rho_{\mathrm{long}}(V_p)$ and $\rho_{\mathrm{trans}}(V_p)$ at $T = 50$ K for a constant field $\mu_0 H = 10$ mT [$\mu_0 H = 100$ mT] applied along $\alpha = -25°$. The data consist of three full voltage cycles ($V_p = +200$ V $\rightarrow$ -200 V $\rightarrow$ $+200$ V) in 5-V steps, evidencing the good reproducibility of the measurement. The hysteresis is due to the hysteretic expansion/contraction of the piezoelectric actuator with V_p [Fig. 4(a)].

Figure 14 shows the magnetization orientation $\beta(V_p)$ as a function of piezo voltage V_p at 50 K obtained from the ρ_{long} data (black open squares) and the ρ_{trans} data (red full circles) for different external magnetic field strengths $\mu_0 H$ applied along $\alpha = -25°$. The abrupt jumps in ρ_{trans} at $V_p \approx -75$ V and $V_p \approx 0$ V for $\mu_0 H = 10$ mT and 20 mT are an artifact of the arcsine transformation caused by the fact that the minimal value of $\rho_{\mathrm{trans}}(V_p \approx 0\ \mathrm{V}) = -0.07$ mΩ cm in Fig. 13(b) is somewhat larger than the value $\frac{1}{2}\rho_7 = -0.1$ mΩ cm in Eq. (3) determined from ADMR traces at 50 K (cf. Fig. 7). The magnetization orientations $\beta(V_p)$ obtained from ρ_{long} and ρ_{trans} consequently are consistent and demonstrate that for $\mu_0 H = 10$ mT we indeed are able to continuously and reversibly adjust the magnetization orientation at will within about 70° solely via application of a voltage to the piezoelectric actuator.[50] With increasing magnetic field strength, the Zeeman contribution in Eq. (1) increasingly dominates over the magnetoelastic contribution to the free energy. Thus the an-

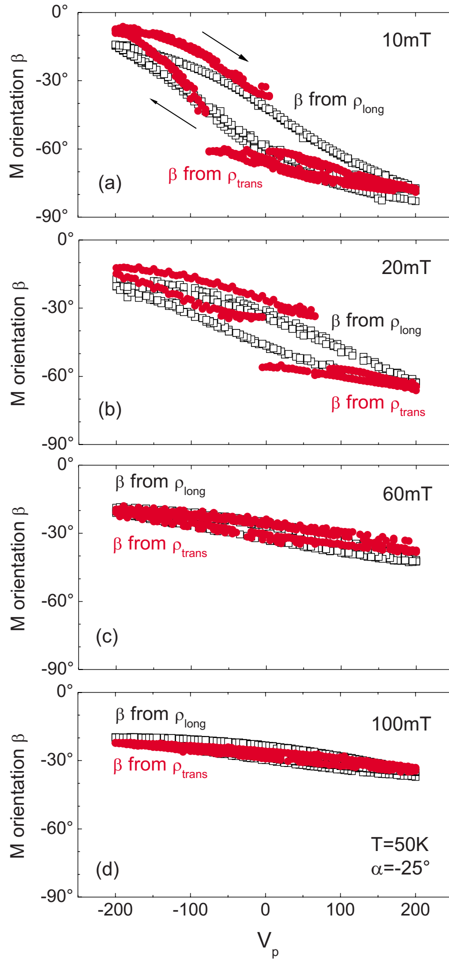

FIG. 14. (Color online) The magnetization orientation β as a function of piezo voltage V_p at 50 K for different external magnetic field strengths $\mu_0 H$ applied along $\alpha = -25°$ calculated from ρ_{long} via Eq. (2) (black open squares) and ρ_{trans} via Eq. (3) (red full circles). The good agreement between the β values calculated from ρ_{long} and ρ_{trans} corroborates our analysis and demonstrates that for $\mu_0 H = 10$ mT, the magnetization orientation can be continuously and reversibly rotated by about $\Delta\beta \approx 70°$ solely by varying the piezo voltage between +200 V and −200 V, as expected from the free energy contours (Fig. 12). For increasing $\mu_0 H$ the maximum angle of rotation is decreased to $\Delta\beta \approx 15°$ for $\mu_0 H = 100$ mT.

gular range within which the magnetization orientation can be rotated as a function of V_p decreases from $\Delta\alpha \approx 70°$ for $\mu_0 H = 10$ mT to $\Delta\alpha \approx 15°$ for $\mu_0 H = 100$ mT.

X. PIEZO VOLTAGE-INDUCED NONVOLATILE MAGNETIZATION SWITCHING

In this section we show that the piezo voltage-induced strain not only allows to control the magnetic anisotropy, but also can be used to induce an irreversible switching of magnetization. The solid black curve in Fig. 15(a) shows the transverse resistivity loop $\rho_{trans}(\mu_0 H)$ at 40 K and $V_p = +200$ V, with the external magnetic field oriented along $\alpha = 335°$. As indicated by the black arrows, $\mu_0 H$ was swept from −300 mT to +300 mT and back to −300 mT. The re-

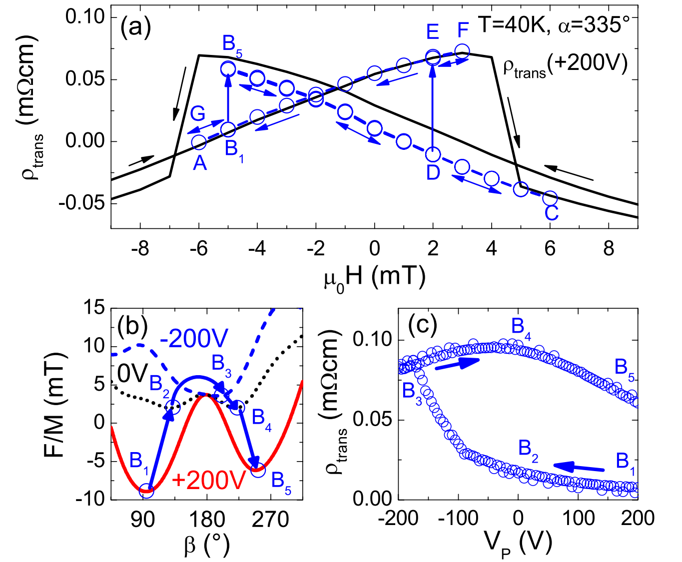

FIG. 15. (Color online) (a) Transverse resistivity loop $\rho_{trans}(\mu_0 H)$ at 40 K with $V_p = +200$ V and the external magnetic field oriented along $\alpha = 335°$. The open blue circles describe the evolution of $\rho_{trans}(\mu_0 H)$ during the measurements sequence A to G described in the text. The fact that the symmetry axis of the full $\rho_{trans}(\mu_0 H)$ loop is not at zero magnetic field, we attribute to trapped flux in the superconducting magnet. (b) Piezo voltage-induced change in free energy normalized on saturation magnetization $F/M(\beta)$ as a function of magnetization orientation β for $\mu_0 H = -5$ mT. (c) Evolution of ρ_{trans} during the piezo voltage sweep from $V_p = +200$ V $(B_1) \to 0$ V $(B_2) \to -200$ V $(B_3) \to 0$ V $(B_4) \to +200$ V (B_5).

sistivity jump in the upsweep at $\mu_0 H \approx +4$ mT is due to a switching of magnetization orientation between two minima in the free energy surface. In the free energy diagram for $\mu_0 H \approx -5$ mT shown in Fig. 15(b), this would correspond to a switching from the minimum at $\beta \approx 90°$ into the minimum at $\beta \approx 250°$. The hysteresis of $\rho_{trans}(\mu_0 H)$ between up- and downsweeps is caused by the magnetization residing in one of these two minima. To induce a switching process of magnetization orientation back to $\beta \approx 90°$, a negative magnetic field in excess of the coercive field $\mu_0 H_C = -6$ mT has to be applied. As we will show in the following, the additional degree of freedom offered by the piezoelectric actuator allows inducing a nonreversible magnetization switching already at external magnetic fields below the coercive field.

Starting from the same magnetic preparation ($\mu_0 H = -300$ mT, $V_p = +200$ V) the upsweep [blue symbols in Fig. 15(a)] is stopped in a second experiment at $\mu_0 H = -5$ mT (position denoted B_1). Keeping the magnetic field constant at this value, the piezo voltage is swept from $V_p = +200$ V to $V_p = -200$ V with the corresponding increase in ρ_{trans} shown in Fig. 15(c) [$B_1(V_p = +200$ V$) \to B_2(V_p = 0$ V$) \to B_3(V_p = -200$ V$)$]. Sweeping the piezo voltage back to $V_p = +200$ V, $\rho_{trans}(\mu_0 H)$ remains in this high resistance state [$B_3(V_p = -200$ V$) \to B_4(V_p = 0$ V$) \to B_5(V_p = +200$ V$)$]. This behavior can be understood with the help of the corresponding free energy plots at $V_p \in \{+200$ V$, 0$ V$, -200$ V$\}$ in Fig. 15(b). These have been derived from ADMR measurements, as described in Sec. V. The free energy plots indicate that the

magnetization orientation is rotated from $\beta \approx 90°$ at $V_p = +200$ V (B_1) over $\beta \approx 135°$ at $V_p = 0$ V (B_2) to $\beta \approx +200°$ at $V_p = -200$ V (B_3). Sweeping V_p back to +200 V, due to the potential barrier at $\beta \approx 180°$, the magnetization does not rotate back in the same way, but evolves into the potential minimum at $\beta \approx +250°$ ($B_3 \rightarrow B_4 \rightarrow B_5$). Therefore, the sweep in piezo voltage from $V_p = +200$ V to $V_p = -200$ V and back to $V_p = +200$ V results in an irreversible magnetization orientation change and the corresponding resistivity change observed at $\mu_0 H = -5$ mT. We note that these experimental results are closely comparable to those reported in manuscript Ref. 51.

Sweeping $\mu_0 H$ from −5 mT to +6 mT ($B_5 \rightarrow C$) after the piezo loop cycling of V_p from +200 V to −200 V and back to +200 V, ρ_{trans} decreases and approximately follows the resistivity curve obtained in the conventional magnetotransport measurement for the opposite sweep direction in this magnetic field range. The fact that ρ_{trans} does not exactly coincide with the downsweep curve, we attribute to first indications of multidomain effects, which begin to become important at these small magnetic fields. In particular, the downsweep curve depicted as the full line in Fig. 15(a) was measured after saturating the magnetization at +300 mT, so that multidomain effects should be less important. As we sweep $\mu_0 H$ back to −5 mT ($C \rightarrow B_5$) and up to +2 mT again ($B_5 \rightarrow D$), ρ_{trans} remains on this resistivity branch.

At $\mu_0 H = +2$ mT (D) we performed a second irreversible switching process via cycling the piezo voltage V_p again from +200 V to −200 V and to +200 V. In analogy to the switching process at −5 mT described above, the magnetization is switched from the minimum at $\beta \approx 250°$ into the minimum at $\beta \approx 90°$ ($D \rightarrow E$). Sweeping $\mu_0 H$ to +3 mT (F) after this second irreversible piezo-induced switching and back to −6 mT (G), ρ_{trans} as expected follows the corresponding upsweep branch. These experiments clearly demonstrate that the piezo voltage not only allows to control the magnetic anisotropy and thus the magnetization orientation, but also to induce an irreversible magnetization switching.

XI. CONCLUSIONS

In summary, we have investigated the magnetic properties of a piezoelectric actuator/ferromagnet hybrid structure. Application of a voltage to the piezoelectric actuator results in an additional uniaxial magnetoelastic contribution to magnetic anisotropy. For the GaMnAs thin film investigated, the axis of elongation (contraction) corresponds to the magnetic hard (easy) axis of this uniaxial magnetic anisotropy. We studied the temperature dependence of the magnetic anisotropy including the magnetoelastic contribution using anisotropic magnetoresistance techniques. The temperature dependence of the derived magnetostrictive constant λ_{111} is in agreement with the first λ_{111} measurements in GaMnAs by Masmanidis *et al.*[27] We explicitly take advantage of the strong temperature dependence of the magnetic anisotropy of GaMnAs to access different regimes of the relative strength of the magnetoelastic and the magnetocrystalline contribution. At $T = 5$ K the magnetoelastic term constitutes only a minor contribution compared to the dominating cubic term, but we showed that the switching fields of $\rho(\mu_0 H)$ loops are shifted by the application of a piezo voltage also at this temperature. At 50 K—where the magnetoelastic term dominates magnetic anisotropy—we demonstrated a continuous, fully reversible control of magnetization orientation by about 70°, solely via application of voltage to the piezoelectric actuator. This piezo voltage control of magnetization orientation is directly transferable to other ferromagnetic/piezoelectric hybrid structures opening the way to new innovative multifunctional device concepts, such as all electrically controlled magnetic memory elements. As an example, the piezo voltage-induced irreversible magnetization switching demonstrated at $T = 40$ K constitutes the basic principle of a nonvolatile memory element. Note that depending on the application intended, care should be taken to adjust the ratio of the magnetoelastic and the magnetocrystalline anisotropy contribution. As exemplarily shown in this paper for a GaMnAs/piezoelectric actuator hybrid sample, in order to maximize the angle of reversible magnetization reorientation, the magnetocrystalline anisotropy contribution should be as small as possible (as, e.g., in polycrystalline soft ferromagnets), while in order to realize a memory device concept based on irreversible magnetization switching, a finite but small magnetocrystalline anisotropy should be present.

XII. OUTLOOK

In this paper, we have demonstrated the manipulation of the magnetization in the plane of a dilute magnetic semiconductor. However, also a manipulation of the magnetization from in-plane to out-of-plane should be possible. For this, the magnetic anisotropy landscape has to be changed by reducing the strong uniaxial anisotropy in growth direction present in $Ga_{1-x}Mn_xAs$ thin films grown on GaAs. As discussed in Sec. I, this can be achieved by growing on a lattice matched $Ga_{1-y}In_yAs$ virtual substrate.[30–32] In the presence of a dominantly cubic magnetic anisotropy with only a small remaining uniaxial anisotropy in growth direction, the application of a biaxial tensile strain within the film plane would thus allow a switching of the magnetization orientation from in-plane to out-of-plane. Such controllable biaxial in-plane strain could be realized, e.g., via cementing the GaMnAs film onto the head side of the piezoelectric actuator. The controlled application of either uniaxial or biaxial stress would allow a full three-dimensional control of the magnetization orientation.

A possible device concept based on this approach is exemplarily illustrated in Fig. 16, consisting of a GaMnAs layer, which is strained locally by a piezo- or ferroelectric actuator. To allow optimal transfer of the stress from the actuator to the DMS layer, the $Ga_{1-x}Mn_xAs$ thin film should be made self-supporting by removing an AlAs sacrificial layer below it via wet-chemical etching. Finally, prestraining of the DMS can be achieved by the $Ga_{1-y}In_yAs$ virtual substrate discussed above or nanopatterning. Of course, since the magnetic anisotropy in GaMnAs in general is not only determined by the biaxial strain, but also additional factors such as hole concentration and temperature,[40] the parameters for the pretailoring of the magnetic anisotropy landscape will

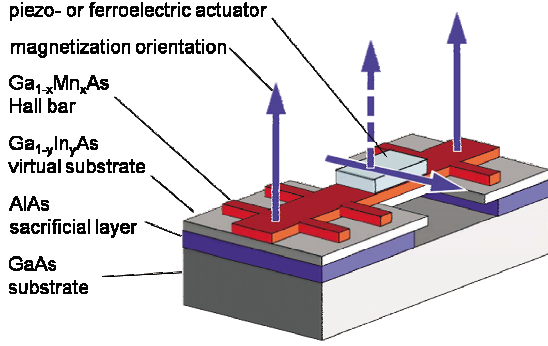

FIG. 16. (Color online) Sketch of a spin valve structure based on strain modulation. The magnetization of the central part of the Hall bar is manipulated by the actuator positioned above a $Ga_{1-x}Mn_xAs$ layer prestrained by a self-supporting $Ga_{1-y}In_yAs$ virtual substrate. In this particular realization, the $Ga_{1-y}In_yAs$ buffer with a lattice constant greater than that of the GaMnAs layer leads to an out-of-plane orientation of the magnetization, which is flipped in-plane by a biaxial compressive strain induced by the actuator.

have to be chosen with care also in the case of in-plane to out-of-plane switching, as has been discussed in detail in this paper for pure in-plane manipulation. To realize efficient strain transducers, a direct deposition of the actuator material onto the DMS is required. The fabrication of standard piezo- or ferroelectrics, such as PZT or $BaTiO_3$, is well established, but typically requires temperatures in excess of 400 °C.[61,62] Therefore, these deposition processes cannot be straightforwardly transferred to GaMnAs films, as this ferromagnetic semiconductor is grown by LT-MBE at substrate temperatures around 250 °C or below.[11] The exposure of GaMnAs to temperatures above 250 °C results in Mn segregation and MnAs formation and thus to a destruction of the ferromagnetic semiconductor. To circumvent this issue, more exotic fabrication routes, e.g., the realization of PZT or $BaTiO_3$ via hydrothermal methods,[63,64] could be viable approaches. Organic ferroelectrics such as poly(vinylidene fluoride/trifluoroethylene) or PVDF/TrFE are interesting alternatives, as they can be spin-coated and polymerized at temperatures below 200 °C and therefore should be compatible with GaMnAs.[65,66]

ACKNOWLEDGMENTS

This work was supported by DFG through SPP 1157, GR 1132/13, and GO 944/3 (Walther-Meissner-Institut), LI 988/4 (Ulm) and SFB 631 (Walter Schottky Institut).

APPENDIX: MAGNETOELASTIC CONTRIBUTION TO MAGNETIC ANISOTROPY ENERGY

In this Appendix we discuss the influence of the piezo voltage-induced strain on the magnetic anisotropy of the film. As described in Sec. III the (001)-oriented sample is cemented onto the piezoelectric actuator with the main expansion direction parallel to the [110] direction of GaAs. In the $\{\mathbf{j},\mathbf{t},\mathbf{n}\}$ coordinate system with $\mathbf{j}\parallel[110]$, $\mathbf{t}\parallel[\bar{1}10]$, and $\mathbf{n}\parallel[001]$, the strain induced by the piezoelectric actuator in the GaMnAs film is given by the tensor

$$\epsilon_{\{\mathbf{j},\mathbf{t},\mathbf{n}\}} = \begin{pmatrix} \epsilon_{jj} & 0 & 0 \\ 0 & \epsilon_{tt} & 0 \\ 0 & 0 & \epsilon_{nn} \end{pmatrix} \tag{A1}$$

with the diagonal components ϵ_{ii} describing the strains along the coordinate axes. Note that all other components vanish since in the $\{\mathbf{j},\mathbf{t},\mathbf{n}\}$ coordinate system, no shear strains are present. To derive the piezo-induced change in magnetic anisotropy, we transform $\epsilon_{\{\mathbf{j},\mathbf{t},\mathbf{n}\}}$ into the $\{\mathbf{x},\mathbf{y},\mathbf{z}\}$ coordinate system with coordinate axes along $\langle 100\rangle$ using the transformation matrix

$$T = \begin{pmatrix} \sqrt{\frac{1}{2}} & \sqrt{\frac{1}{2}} & 0 \\ -\sqrt{\frac{1}{2}} & \sqrt{\frac{1}{2}} & 0 \\ 0 & 0 & 1 \end{pmatrix} \tag{A2}$$

and its inverted matrix

$$T^{-1} = \begin{pmatrix} \sqrt{\frac{1}{2}} & -\sqrt{\frac{1}{2}} & 0 \\ \sqrt{\frac{1}{2}} & \sqrt{\frac{1}{2}} & 0 \\ 0 & 0 & 1 \end{pmatrix}. \tag{A3}$$

In this way we obtain the strain tensor in the $\{\mathbf{x},\mathbf{y},\mathbf{z}\}$ coordinate system:

$$\epsilon_{\{\mathbf{x},\mathbf{y},\mathbf{z}\}} = T\epsilon_{\{\mathbf{j},\mathbf{t},\mathbf{n}\}}T^{-1} = \begin{pmatrix} \frac{1}{2}(\epsilon_{jj}+\epsilon_{tt}) & -\frac{1}{2}(\epsilon_{jj}-\epsilon_{tt}) & 0 \\ -\frac{1}{2}(\epsilon_{jj}-\epsilon_{tt}) & \frac{1}{2}(\epsilon_{jj}+\epsilon_{tt}) & 0 \\ 0 & 0 & \epsilon_{nn} \end{pmatrix} \tag{A4}$$

with the strains $\epsilon_{xx}=\epsilon_{yy}=\frac{1}{2}(\epsilon_{jj}+\epsilon_{tt})$ and $\epsilon_{zz}=\epsilon_{nn}$ and the shear strains $\epsilon_{xy}=\epsilon_{yx}=-\frac{1}{2}(\epsilon_{jj}-\epsilon_{tt})$. These are now inserted in the general expression for the magnetoelastic contribution to the magnetic anisotropy[67]

$$F_{\text{magel}} = B_1\left[\epsilon_{xx}\left(m_x^2-\frac{1}{3}\right)+\epsilon_{yy}\left(m_y^2-\frac{1}{3}\right)+\epsilon_{zz}\left(m_z^2-\frac{1}{3}\right)\right] + B_2(\epsilon_{xy}m_xm_y+\epsilon_{yz}m_ym_z+\epsilon_{xz}m_zm_x) \tag{A5}$$

with m_i denoting the direction cosines of magnetization orientation with respect to the cubic axes, the magnetoelastic coupling constants B_i, and ϵ_{ij} describing the strains in the $\{\mathbf{x},\mathbf{y},\mathbf{z}\}$ coordinate system. The magnetoelastic coupling constants B_i can be substituted with the magnetostrictive constants λ_{100} and λ_{111} using the relations $B_1=\frac{3}{2}\lambda_{100}(c_{12}-c_{11})$ and $B_2=-3\lambda_{111}c_{44}$ with the elastic moduli c_{ij}.[7]

Since $\epsilon_{xx}=\epsilon_{yy}$, $m_x^2+m_y^2=1$, and magnetization is oriented in the film plane ($m_z=0$), the first term in Eq. (A5) exhibits no anisotropy and therefore in the following is omitted. Fur-

thermore, using $m_x m_y = \cos(\beta+45°)\cos(\beta-45°) = \cos^2(\beta) - \frac{1}{2}$ and again omitting the isotropic part we obtain

$$F_{\mathrm{magel}}/M = \frac{3\lambda_{111}c_{44}(\epsilon_{jj}-\epsilon_{tt})}{2M}\cos^2\beta = B_{110}m_j^2. \quad \text{(A6)}$$

This expression constitutes a uniaxial magnetic anisotropy contribution along [110] with the direction cosine of magnetization orientation relative to the **j** axis m_j and the corresponding uniaxial anisotropy parameter $B_{110} = 3\lambda_{111}c_{44}(\epsilon_{jj} - \epsilon_{tt})/2M$ and is used as the third term in the total free energy in Eq. (1).

---

*Christoph.Bihler@wsi.tum.de
†Matthias.Althammer@wmi.badw-muenchen.de
‡Sebastian.Goennenwein@wmi.badw-muenchen.de

[1] H. Ohno, Science **281**, 951 (1998).
[2] T. Dietl, H. Ohno, F. Matsukura, J. Cibert, and D. Ferrand, Science **287**, 1019 (2000).
[3] S. A. Wolf, D. D. Awschalom, R. A. Buhrman, J. M. Daughton, S. v. Molnár, M. L. Roukes, A. Y. Chtchelkanova, and D. M. Treger, Science **294**, 1488 (2001).
[4] C. Rüster, T. Borzenko, C. Gould, G. Schmidt, L. W. Molenkamp, X. Liu, T. J. Wojtowicz, J. K. Furdyna, Z. G. Yu, and M. E. Flatté, Phys. Rev. Lett. **91**, 216602 (2003).
[5] S. J. Pearton, D. P. Norton, R. Frazier, S. Y. Han, C. R. Abernathy, and J. M. Zavada, IEE Proc.: Circuits Devices Syst. **152**, 312 (2005).
[6] T. Jungwirth, J. Sinova, J. Mašek, J. Kučera, and A. H. MacDonald, Rev. Mod. Phys. **78**, 809 (2006).
[7] T. Figielski, T. Wosinski, A. Morawski, A. Makosa, J. Wrobel, and J. Sadowski, Appl. Phys. Lett. **90**, 052108 (2007).
[8] K. Pappert, S. Hümpfner, C. Gould, J. Wenisch, K. Brunner, G. Schmidt, and L. W. Molenkamp, Nat. Phys. **3**, 573 (2007).
[9] T. Dietl, H. Ohno, and F. Matsukura, Phys. Rev. B **63**, 195205 (2001).
[10] H. X. Tang, R. K. Kawakami, D. D. Awschalom, and M. L. Roukes, Phys. Rev. Lett. **90**, 107201 (2003).
[11] H. Ohno and F. Matsukura, Solid State Commun. **117**, 179 (2001).
[12] P. Van Dorpe, Z. Liu, W. Van Roy, V. F. Motsnyi, M. Sawicki, G. Borghs, and J. De Boeck, Appl. Phys. Lett. **84**, 3495 (2004).
[13] J. G. Braden, J. S. Parker, P. Xiong, S. H. Chun, and N. Samarth, Phys. Rev. Lett. **91**, 056602 (2003).
[14] M. Tanaka and Y. Higo, Phys. Rev. Lett. **87**, 026602 (2001).
[15] U. Welp, V. K. Vlasko-Vlasov, X. Liu, J. K. Furdyna, and T. Wojtowicz, Phys. Rev. Lett. **90**, 167206 (2003).
[16] Y. Ohno, D. K. Young, B. Beschoten, F. Matsukura, H. Ohno, and D. D. Awschalom, Nature (London) **402**, 790 (1999).
[17] M. Yamanouchi, D. Chiba, F. Matsukura, and H. Ohno, Nature (London) **428**, 539 (2004).
[18] M. Yamanouchi, D. Chiba, F. Matsukura, T. Dietl, and H. Ohno, Phys. Rev. Lett. **96**, 096601 (2006).
[19] C. Gould, C. Rüster, T. Jungwirth, E. Girgis, G. M. Schott, R. Giraud, K. Brunner, G. Schmidt, and L. W. Molenkamp, Phys. Rev. Lett. **93**, 117203 (2004).
[20] H. Ohno, D. Chiba, F. Matsukura, T. Omiya, E. Abe, T. Dietl, Y. Ohno, and K. Ohtani, Nature (London) **408**, 944 (2000).
[21] D. Chiba, M. Yamanouchi, F. Matsukura, and H. Ohno, Science **301**, 943 (2003).
[22] S. Koshihara, A. Oiwa, M. Hirasawa, S. Katsumoto, Y. Iye, C. Urano, H. Takagi, and H. Munekata, Phys. Rev. Lett. **78**, 4617 (1997).
[23] H. Boukari, P. Kossacki, M. Bertolini, D. Ferrand, J. Cibert, S. Tatarenko, A. Wasiela, J. A. Gaj, and T. Dietl, Phys. Rev. Lett. **88**, 207204 (2002).
[24] X. Liu *et al.*, Physica E (Amsterdam) **20**, 370 (2004).
[25] K. Hamaya, T. Taniyama, Y. Kitamoto, R. Moriya, and H. Munekata, J. Appl. Phys. **94**, 7657 (2003).
[26] M. Sawicki *et al.*, Phys. Rev. B **71**, 121302(R) (2005).
[27] S. C. Masmanidis, H. X. Tang, E. B. Myers, M. Li, K. De Greve, G. Vermeulen, W. V. Roy, and M. L. Roukes, Phys. Rev. Lett. **95**, 187206 (2005).
[28] L. V. Titova, M. Kutrowski, X. Liu, R. Chakarvorty, W. L. Lim, T. Wojtowicz, J. K. Furdyna, and M. Dobrowolska, Phys. Rev. B **72**, 165205 (2005).
[29] K. Takamura, F. Matsukura, D. Chiba, and H. Ohno, Appl. Phys. Lett. **81**, 2590 (2002).
[30] X. Liu, Y. Sasaki, and J. K. Furdyna, Phys. Rev. B **67**, 205204 (2003).
[31] X. Liu, W. L. Lim, L. V. Titova, M. Dobrowolska, J. K. Furdyna, M. Kutrowski, and T. Wojtowicz, J. Appl. Phys. **98**, 063904 (2005).
[32] A. Shen, H. Ohno, F. Matsukura, Y. Sugawara, N. Akiba, T. Kuroiwa, A. Oiwa, A. Endo, S. Katsumota, and Y. Iye, J. Cryst. Growth **175-176**, 1069 (1997).
[33] J. Daeubler, S. Schwaiger, M. Glunk, M. Tabor, W. Schoch, R. Sauer, and W. Limmer, Physica E (Amsterdam) **40**, 1876 (2008).
[34] M. Csontos, G. Mihály, B. Jankó, T. Wojtowicz, X. Liu, and J. K. Furdyna, Nat. Mater. **4**, 447 (2005).
[35] S. T. B. Goennenwein, T. A. Wassner, H. Huebl, M. S. Brandt, J. B. Philipp, M. Opel, R. Gross, A. Koeder, W. Schoch, and A. Waag, Phys. Rev. Lett. **92**, 227202 (2004).
[36] R. Bouanani-Rahbi, B. Clerjaud, B. Theys, A. Lemaître, and F. Jomard, Physica B (Amsterdam) **340-342**, 284 (2003).
[37] M. S. Brandt *et al.*, Appl. Phys. Lett. **84**, 2277 (2004).
[38] L. Thevenard, L. Largeau, O. Mauguin, A. Lemaître, and B. Theys, Appl. Phys. Lett. **87**, 182506 (2005).
[39] R. Farshchi, O. D. Dubon, D. J. Hwang, N. Misra, C. P. Grigoropoulos, and P. D. Ashby, Appl. Phys. Lett. **92**, 012517 (2008).
[40] M. Sawicki, F. Matsukura, A. Idziaszek, T. Dietl, G. M. Schott, C. Ruester, C. Gould, G. Karczewski, G. Schmidt, and L. W. Molenkamp, Phys. Rev. B **70**, 245325 (2004).
[41] U. Welp, V. K. Vlasko-Vlasov, A. Menzel, H. D. You, X. Liu, J. K. Furdyna, and T. Wojtowicz, Appl. Phys. Lett. **85**, 260 (2004).
[42] V. Stanciu and P. Svedlindh, Appl. Phys. Lett. **87**, 242509 (2005).
[43] K. Hamaya, T. Taniyama, Y. Kitamoto, T. Fujii, and Y. Yamazaki, Phys. Rev. Lett. **94**, 147203 (2005).
[44] K. Y. Wang, K. W. Edmonds, L. X. Zhao, M. Sawicki, R. P.

Campion, B. L. Gallagher, and C. T. Foxon, Phys. Rev. B **72**, 115207 (2005).
[45] K. Hamaya, T. Koike, T. Taniyama, T. Fujii, Y. Kitamoto, and Y. Yamazaki, Phys. Rev. B **73**, 155204 (2006).
[46] K. Hamaya, T. Watanabe, T. Taniyama, A. Oiwa, Y. Kitamoto, and Y. Yamazaki, Phys. Rev. B **74**, 045201 (2006).
[47] J. Wenisch, C. Gould, L. Ebel, J. Storz, K. Pappert, M. J. Schmidt, C. Kumpf, G. Schmidt, K. Brunner, and L. W. Molenkamp, Phys. Rev. Lett. **99**, 077201 (2007).
[48] B. Botters, F. Giesen, J. Podbielski, P. Bach, G. Schmidt, L. W. Molenkamp, and D. Grundler, Appl. Phys. Lett. **89**, 242505 (2006).
[49] A. Brandlmaier *et al.*, Phys. Rev. B **77**, 104445 (2008).
[50] S. T. B. Goennenwein, M. Althammer, C. Bihler, A. Brandlmaier, S. Geprägs, M. Opel, W. Schoch, W. Limmer, R. Gross, and M. S. Brandt, Phys. Status Solidi (RRL) **2**, 96 (2008).
[51] A. W. Rushforth *et al.*, arXiv:0801.0886 (unpublished).
[52] M. Overby, A. Chernyshov, L. P. Rokhinson, X. Liu, and J. K. Furdyna, Appl. Phys. Lett. **92**, 192501 (2008).
[53] W. Limmer, M. Glunk, J. Daeubler, T. Hummel, W. Schoch, R. Sauer, C. Bihler, H. Huebl, M. S. Brandt, and S. T. B. Goennenwein, Phys. Rev. B **74**, 205205 (2006).
[54] W. Limmer, J. Daeubler, L. Dreher, M. Glunk, W. Schoch, S. Schwaiger, and R. Sauer, Phys. Rev. B **77**, 205210 (2008).
[55] C. Bihler, H. Huebl, M. S. Brandt, S. T. B. Goennenwein, M. Reinwald, U. Wurstbauer, M. Döppe, D. Weiss, and W. Wegscheider, Appl. Phys. Lett. **89**, 012507 (2006).
[56] C. Bihler, M. Kraus, H. Huebl, M. S. Brandt, S. T. B. Goennenwein, M. Opel, M. A. Scarpulla, P. R. Stone, R. Farshchi, and O. D. Dubon, Phys. Rev. B **75**, 214419 (2007).
[57] T. Yamada, D. Chiba, F. Matsukura, S. Yakata, and H. Ohno, Phys. Status Solidi C **3**, 4086 (2006).
[58] S. T. B. Goennenwein, S. Russo, A. F. Morpurgo, T. M. Klapwijk, W. Van Roy, and J. De Boeck, Phys. Rev. B **71**, 193306 (2005).
[59] D. Wu, P. Wei, E. Johnston-Halperin, D. D. Awschalom, and J. Shi, Phys. Rev. B **77**, 125320 (2008).
[60] J. S. Blakemore, J. Appl. Phys. **53**, R123 (1982).
[61] M. Matsuoka, K. Hoshino, and K. Ono, J. Appl. Phys. **76**, 1768 (1994).
[62] M. Alexe and D. Hesse, J. Mater. Sci. **41**, 1 (2006).
[63] T. Morita, Y. Wagatsuma, Y. Cho, H. Morioka, H. Funakubo, and N. Setter, Appl. Phys. Lett. **84**, 5094 (2004).
[64] T. Morita and Y. Cho, Appl. Phys. Lett. **88**, 112908 (2006).
[65] T. Furukawa, Phase Transitions **18**, 143 (1989).
[66] R. C. G. Naber, C. Tanase, P. W. M. Blom, G. H. Gelinck, A. W. Marsman, F. J. Touslager, S. Setayesh, and D. M. De Leeuw, Nat. Mater. **4**, 243 (2005).
[67] S. Chikazumi, *Physics of Magnetism* (Wiley, New York, 1964).